Available online at www.sciencedirect.com
ScienceDirect
Journal of Volcanology and Geothermal Research 164 (2007) 112–126
Journal of volcanology and geothermal research
www.elsevier.com/locate/jvolgeores

Statistical analysis of bubble and crystal size distributions: Application to Colorado Plateau basalts

Alexander A. Proussevitch [a], Dork L. Sahagian [b,*], William D. Carlson [c]

[a] Climate Change Research Center and Department of Earth Sciences, University of New Hampshire, Durham, NH 03824, United States
[b] Department of Earth & Environmental Sciences, and the Environmental Initiative, Lehigh University, Bethlehem, PA 18015, United States
[c] Department of Geological Sciences, University of Texas at Austin, Austin, TX 78712, United States

Received 12 April 2006; received in revised form 7 February 2007; accepted 13 April 2007
Available online 10 May 2007

Abstract

A new analytical technique for the statistical analysis of bubble populations in volcanic rocks [Proussevitch, A.A., Sahagian, D.L. and Tsentalovich, E.P., 2007-this issue. Statistical analysis of bubble and crystal size distributions: Formulations and procedures. J. Volc. Geotherm. Res.] has been applied to a collection of Colorado Plateau basalts (96 samples). A variety of mono- and polymodal distributions has been found in the samples, all of which belong to the logarithmic family of statistical functions. Most samples have bimodal log normal distributions, while the others are represented by mono- or bimodal log logistic, and Weibull distributions. We have grouped the observed distributions into 11 groups depending on distribution types, mode location, and intensity. The nature of the curves within these groups can be interpreted as evolution of vesiculation processes. We conclude that within bimodal log normal distributions, the mode of smaller bubbles is the result of a second nucleation and growth event in a lava flow after eruption. In the case of log logistic distributions the larger mode results from coalescence of bubbles. Coalescence processes are reflected in growth of a larger mode and decreasing bubble number density. Another style of population evolution leads to a monomodal Weibull (or exponential) distribution as a result of superposition of multiple log normal distributions in which the modes are comparable in size and intensity. These various population distribution styles can be interpreted with an understanding of vesiculation processes that can be gained through appropriate numerical models of coalescence and population evolution. The applicable vesiculation processes include: a) a single nucleation-growth event, b) continuous multiple nucleation-growth events, c) coalescence, and d) Ostwald ripening.
Published by Elsevier B.V.

Keywords: bubble and crystal size distribution; statistical analysis; bubble number density; crystal number density; exceedance; magma chamber processes; eruption dynamics; vesicular basalts

1. Introduction

Interest in bubble size distributions in volcanic rocks has recently intensified because it has been recognized that they contain critical information about magma history and physical processes at the vent as well as within surface lava flows (Gaonac'h et al., 1996b; Cashman and Kauahikaua, 1997; Blower et al., 2001; Blower et al., 2003; Shin et al., 2005).

* Corresponding author.
E-mail addresses: alex.proussevitch@unh.edu (A.A. Proussevitch), dork.sahagian@lehigh.edu (D.L. Sahagian), wcarlson@mail.utexas.edu (W.D. Carlson).

0377-0273/$ - see front matter. Published by Elsevier B.V.
doi:10.1016/j.jvolgeores.2007.04.006

Studies of bubble size distributions have not been systematic because they have been limited by two major factors:

1. Poor data collection (analytical) techniques (mostly image analysis of 2D cross-sections) that cannot provide representative numbers of bubbles within a population, and have been prone to 2D–3D conversion problems (Sahagian and Proussevitch, 1998). Furthermore, these techniques have not been capable of detecting relatively small bubbles.
2. Lack of a robust statistical approach that would enable the characterization of bubble populations in terms of distribution functions and their spatial characteristics.

The present study was directed to overcome these two major impediments to bubble population analysis. The former was addressed by high-resolution X-ray computed tomography (HRXCT) and is described in Section 3. A solution for the latter was suggested by (Proussevitch et al., 2007-this issue). In this paper, we apply a newly developed technique to a suite of 96 vesicular basalt samples collected from 50 sites of the Colorado Plateau (Section 2) for the purpose of constraining plateau uplift history. These samples provide a robust demonstration of the power of our new analytical and statistical techniques in determining the fundamental relations between the physical processes of vesiculation and resulting bubble populations in volcanic rocks. This approach is not limited to bubbles, but should also be applicable to studies of crystal size distributions, particles in sedimentary rocks, etc.

The analysis of Colorado Plateau basalts resulted in a variety of mono- and polymodal distribution types that have been grouped (Section 5.3) and speculatively interpreted from the standpoint of alternative scenarios of vesiculation processes (Section 5.4) such as single nucleation and bubble growth event, multiple nucleation events, and coalescence.

One of the most fundamental results of this work is that all bubble size distributions belong to the logarithmic family of statistical distributions and of these, most are log normal. Other logarithmic family functions (logistic, Weibull, and exponential) are also found, but are less common (Sections 4 and 5).

The analytical approach developed here has many advantages over previous studies. There have been some analytical functions reported to describe bubble populations, such as exponential (Marsh, 1988; Cashman and Mangan, 1994), log normal (Sarda and Graham, 1990; Shin et al., 2005), and power (Gaonac'h et al., 1996a,b). However, until now it has not been understood how each of these fits within a single family of statistical distributions. Moreover, the power function is an approximation of the upper asymptote of the Weibull distribution for large bubbles that results when the smaller bubbles in the distributions are not included in the observational data (Proussevitch et al., 2007-this issue).

An important parameter in bubble distributions is Bubble Number Density (BND). There has been some confusion and misunderstanding of BND definition in the traditional volcanological literature that has resulted from erroneously treating bubbles like crystals. Because the molar volume of gas in bubbles is vastly greater than that of melt. BND must be defined as bubbles per volume of melt, not volume of bulk magma. We demonstrate that BND is a direct product of the statistical analysis as being one of the coefficients in all distribution functions (Proussevitch et al., 2007-this issue).

2. Sample collection

We have analyzed a collection of 96 samples of Cenozoic basalts from the Colorado Plateau (Fig. 1). All samples were collected in pairs from quenched crusts at the top and bottom of lava flows for analysis leading to paleoelevation and uplift history (Sahagian et al., 2002a,b). The collection also ideally suited for a complete statistical analysis of bubble populations.

Fig. 1 shows the localities sampled around the margin of the Plateau and represented mostly by Oligocene to

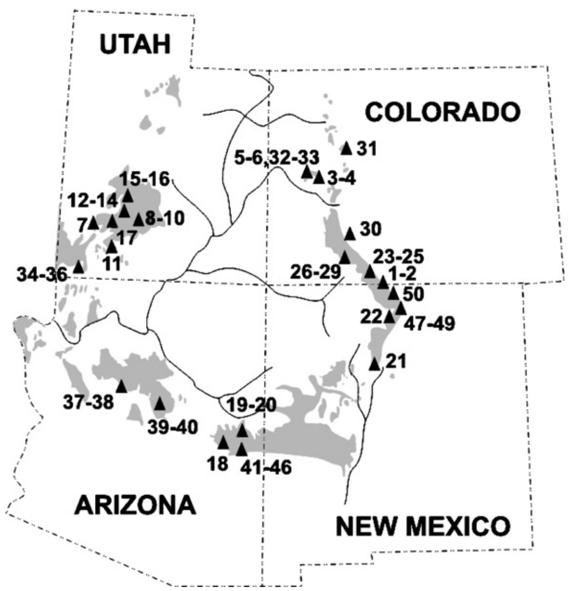

Fig. 1. Sample localities of Colorado Plateau basalt from the collection. Cenozoic lava fields are shaded. Sample numbers correspond to those of Table 1.

Miocene volcanic formations with composition ranging from andesites to olivine basalts. Younger Miocene to Quaternary basalts tended to be around the Southern margin and represented by continental tholeiitic basalts. Accordingly the basalt samples have been collected from these volcanic fields but not differentiated by age or petrology since the focus of this study is bubble size distribution statistics.

3. Sample analysis

In order to conduct the statistical analysis, we needed to produce bubble population data for each sample, consisting of a dataset of individual bubble sizes (volumes) in the sample. We used high-resolution X-ray computed tomography (HRXCT) imagery that then had been processed by object recognition procedures developed previously (Proussevitch and Sahagian, 2001). These two steps can be summarized as follows:

HRXCT was performed at the University of Texas at Austin using an instrument and protocols developed specifically for geoscience applications (Ketcham and Carlson, 2001). A cylindrical core 24mm in diameter was drilled from each sample and scanned to produce 3-dimensional array of attenuation measurements with dimensions of either $512\times512\times351$ or $1024\times1024\times696$; corresponding spatial resolutions were 46.9µm and 23.4µm respectively. The larger arrays were re-sampled to $512\times512\times348$, in order to make the resolution equivalent to that in the other scans (46.9µm), and to reduce the overall size of the data set to facilitate processing by the size-analysis software.

X-ray attenuation is directly related to local mass density in the sample, allowing the dataset to be segmented in order to differentiate solid material from voids. We used a kriging thresholding algorithm to perform the segmentation (Oh and Lindquist, 1999), employing a moving window semivariogram of 10 voxels maximum lag distance. The segmented data were processed by a "peeling" technique for convex object recognition (Proussevitch and Sahagian, 2001).

The resulting dataset of bubble population included $\sim 10^4$ bubbles in each sample and represents a very detailed bubble size data. Individual bubble sizes in the datasets ranged from about 0.1 to ~ 3 millimeters in diameter.

4. Statistical analysis of bubble populations

The mathematical background and some critical details of the statistical analysis are described in a companion paper (Proussevitch et al., 2007-this issue). A flowchart of the analysis represents the logical flow of the procedure (Fig. 2).

The analysis basically involved three stages. First, bubble size data was aggregated to statistical values. To generate distribution density and associated error estimates we applied Log_{10} based volume unit conversion so that linear distribution functions could be used in the next stage. However, for exceedance we did not use unit

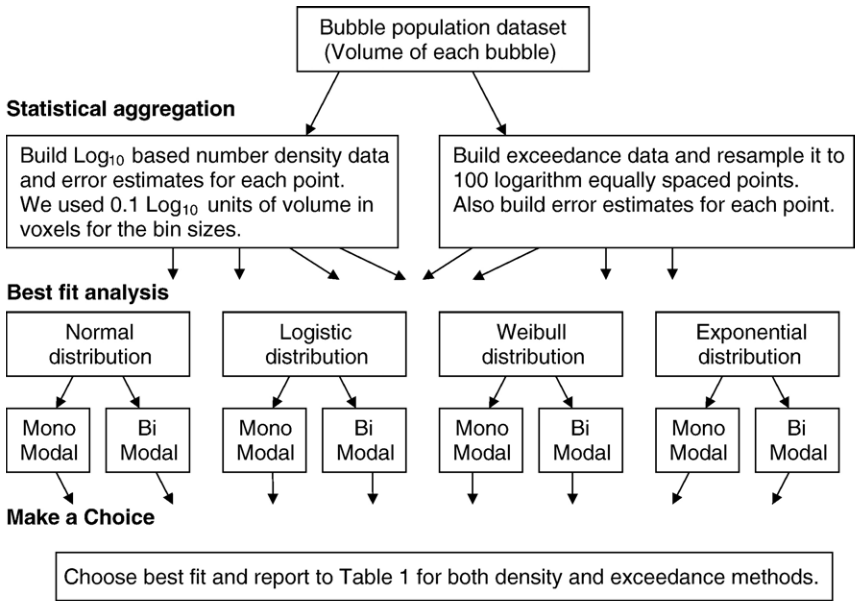

Fig. 2. Flowchart of statistical analysis of bubble population data for each sample.

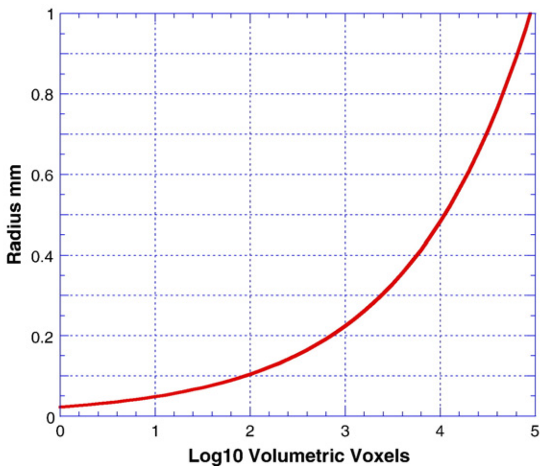

Fig. 3. Conversion of Log10 volumetric voxels used in this paper for bubble sizes to radius in mm.

conversions since exceedance functions are not available in analytical form for any distributions except normal.

In the second stage, the best fit analysis was performed for both probability density and exceedance. Normal, logistic, Weibull, and exponential distribution functions were tested for mono- and bimodal types and for both density and exceedance data, making 16 tests for each of the samples (see Fig. 3).

While the first two stages were formal and were performed by a set of numerical codes combined in executable scripts, the last stage involved a "human" factor in making the best choice based on combination of minimal chi-square values for each fit, visual assessment of mono- or bimodal probability density graph, and resulting data consistency for both probability density and exceedance methods. The latter is quite important since the exceedance method potentially provides more accurate numbers but is prone to failure if more than 40% of the total bubble population is missing from the data due to observational limitations (see discussion in (Proussevitch et al., 2007-this issue)). Typically, the type of distribution for samples from top and bottom of the same lava flow matched, lending some credence to the interpretation that the distributions reflect vesiculation processes.

The best fit results for all available samples are summarized in Table 1[1].

[1] Here in Table 1 and thereafter in the paper all bubble sizes, statistical modes, etc. are given in Log10 volumetric voxel units. Please, consult Fig. 3 for conversion.

5. Results and discussion

Table 2 indicates that most of the samples have normal[2] distributions (70 counts) while logistic and Weibull distributions have 17 and 9 counts respectively. There are twice as many bimodal distributions than monomodal. Note that all of the Weibull distributions are monomodal.

5.1. Best fit confidence

A critical aspect of the interpretation is how well the various distribution functions fit the actual data. Fig. 4 compares chi-square[3] values obtained from all four functions. Since there are no robust confidence level estimates for chi-square fits, we used a threshold value for chi-square equal to 3 to differentiate between good and poor fits. According to this criterion, good fits are those that lie within about 1.7 measurement standard deviation distances from the actual data points. While it is a subjective value, it has a very good visual fit to the actual data (Fig. 5).

Fig. 4 indicates that normal and logistic distributions are very similar. Quite often it is just a matter of researcher preference as to which one to choose since fit errors are virtually identical. This is illustrated in Fig. 4 by a note indicating that actual data could be fit by both functions, but the one with smaller chi-square is preferable. Note also that most of the samples could be approximated by these functions. Further, there is no exponential distribution that fits better than Weibull, illustrating the fact that exponential distribution is just a special case of Weibull with sigma equal to 1 (Proussevitch et al., 2007-this issue) and the samples that lie along the diagonal have this value.

Fig. 6 shows a histogram of chi-square values differentiated by distribution type. It is evident that almost all samples have a good fit under the chi-square threshold value.

5.2. Distribution parameters

There are three basic parameters for each of the best fit distribution types. These are distribution sigma, position of mode, and BND. If a distribution is bimodal,

[2] Here and thereafter we omit "log" prefix from all distribution names since all of them belong to logarithmic family.

[3] Here and thereafter we refer chi-square as its normalized value to degrees of freedom. This way its value shows how close it follows observation points, and deviation distance is measured by a unit of observation error (sigma).

Table 1
Best fit functions of statistical distributions for bubble populations in basalt samples from Colorado Plateau

Sample	Mode 1			Mode 2			Mean χ^2	Void Fraction, %		Method	Distribution
	s	*v*	BND, 10^9 or fraction	σ	*v*	BND, 10^9 or fraction		Observed	Calculated		
01t	0.801	1.223	0.292	0.503	3.617	0.154	1.145	13.799	11.583	Density	Normal
	1.057	0.948	0.738	0.484	3.667	0.262	0.467*	-	-	Exceedance	
02t	0.464	1.385	1.079	0.255	2.812	0.235	1.731	7.097	-	Density	Logistic
	0.508	1.290	0.830	0.268	2.752	0.170	2.692*	-	-	Exceedance	
05b	0.852	0.447	0.403	0.225	3.640	0.091	1.609	9.823	-	Density	Logistic
06t	1.237	2.494	0.170	0.412	4.360	0.034	0.611	26.466	30.567	Density	Normal
	1.447	2.555	0.892	0.364	4.298	0.108	0.186*	-	-	Exceedance	
07b	1.105	1.678	0.384	–	–	–	1.071	4.089	4.590	Density	Normal
	1.106	1.684	1.000	–	–	–	0.772*	-	-	Exceedance	
07t	0.984	1.811	0.311	0.421	2.793	0.205	0.740	4.304	4.576	Density	Normal
	1.026	1.743	0.596	0.428	2.782	0.404	0.150*	-	-	Exceedance	
11t	0.535	1.492	2.811	–	–	–	2.085	16.804	-	Density	Logistic
	0.567	1.394	1.000	–	–	–	5.442*	-	-	Exceedance	
13t	1.300	1.791	0.198	0.482	4.077	0.093	0.799	21.332	24.392	Density	Normal
	1.300	1.797	0.680	0.475	4.084	0.320	0.094*	-	-	Exceedance	
14t	0.758	1.613	0.271	0.575	3.415	0.232	1.666	14.338	13.368	Density	Normal
	1.035	1.630	0.666	0.530	3.517	0.334	0.595*	-	-	Exceedance	
17b	–	–	–	0.663	2.833	2.185	4.375	17.944	17.181	Density	Weibull
	–	–	–	0.643	2.834	1.000	5.022*	-	-	Exceedance	
18b	2.646	0.728	0.508	–	–	–	1.070	13.260	19.379	Density	Weibull
	2.624	0.864	1.000	–	–	–	0.339*	-	-	Exceedance	
21t	0.386	1.546	1.309	0.322	4.112	0.080	1.731	20.164	27.565	Density	Logistic
	0.455	1.402	0.963	0.227	4.261	0.037	6.837*	-	-	Exceedance	
22b	–	–	–	0.972	2.164	1.504	2.479	21.037	21.692	Density	Normal
	–	–	–	1.010	2.126	1.000	1.909*	-	-	Exceedance	
23b	0.654	1.395	0.570	0.647	4.390	0.079	1.504	33.830	37.819	Density	Normal
	0.570	1.438	0.856	0.726	4.233	0.144	1.536*	-	-	Exceedance	
25t	0.451	1.282	1.243	–	–	–	1.582	20.877	13.446	Density	Logistic
	0.534	0.935	1.000	–	–	–	9.242*	-	-	Exceedance	
26b	0.886	1.246	2.122	–	–	–	4.831	3.026	2.989	Density	Normal
	0.922	1.166	1.000	–	–	–	12.158*	-	-	Exceedance	
27t	1.216	2.572	1.375	–	–	–	2.143	19.049	19.871	Density	Weibull
	1.269	2.530	1.000	–	–	–	3.584*	-	-	Exceedance	
31b	0.344	1.539	0.436	0.357	3.329	0.245	1.759	19.831	21.114	Density	Logistic
	0.390	1.504	0.667	0.367	3.353	0.333	1.358*	-	-	Exceedance	
31t	0.671	1.815	0.170	0.643	3.902	0.202	0.899	33.773	33.313	Density	Normal
	0.717	1.819	0.472	0.629	3.926	0.528	0.099*	-	-	Exceedance	
32b	–	–	–	0.929	3.016	0.392	1.170	25.243	29.171	Density	Normal
	–	–	–	0.926	3.023	1.000	0.463*	-	-	Exceedance	
37b	0.942	2.021	0.805	0.497	3.536	0.467	1.252	29.114	29.054	Density	Normal
	0.970	2.015	0.642	0.497	3.541	0.358	0.222*	-	-	Exceedance	
37t	0.709	1.530	0.397	0.77	3.581	0.270	0.913	28.691	34.088	Density	Normal
	0.852	1.500	0.661	0.733	3.672	0.339	0.543*	-	-	Exceedance	
38b	1.08	2.371	0.309	0.489	3.604	0.055	0.775	41.422	17.153	Density	Normal
	0.905	2.004	0.599	0.719	3.436	0.401	0.063*	-	-	Exceedance	
38t	0.704	1.680	0.913	0.642	3.876	0.212	1.327	32.281	33.563	Density	Normal
	0.727	1.672	0.822	0.619	3.909	0.178	0.806*	-	-	Exceedance	
44t	0.396	1.692	0.378	0.398	4.019	0.069	0.991	23.326	-	Density	Logistic
	0.431	1.646	0.862	0.364	4.064	0.138	0.886*	-	-	Exceedance	
46b	0.767	1.682	0.380	0.648	3.839	0.116	1.171	20.562	20.661	Density	Normal
	0.760	1.677	0.755	0.671	3.828	0.245	0.344*	-	-	Exceedance	

*Chi-square is not adjusted for exceedance rescaling, and so not reliable. 100 sample points were used for function fit.

then it has two sets of these parameters. The values of the three parameters can be obtained by fitting either probability density or exceedance (Table 1), and the values should be similar in either case. Indeed, Fig. 7 indicates a very good match of the values obtained by the two methods. Keep in mind that the third parameter

Table 2
Summary of best fit results presented in Table 1

Distribution	Mono-modal	Bimodal	Total
Normal	18	52	70
Logistic	6	11	17
Weibull	9	–	9
Exponential	–	–	–
All	33	63	96

(BND) cannot be obtained from exceedance, but is a product of the number density function (Proussevitch et al., 2007-this issue).

Fig. 7 also displays histograms of the parameters which indicate a rather wide range of sigma and a bimodal character of distribution modal positions. Thus there are two distinctive bubble size modes. The first mode (small bubbles) varies from 1 to its peak at 1.75 and then to 2.5 in units of Log10 voxels (diameters of 50, 85 and 150µm respectively). The second mode varies from 3 to its peak at 3.75 and then to 4.5 Log10 voxels (diameters of 225, 400 and 710µm respectively). It is interesting that all bimodal distributions in our samples have the two modes in these ranges (Table 1). Most monomodal distributions have their single mode within the first range. This suggests that the second mode is derived from the first during maturation of the distribution.

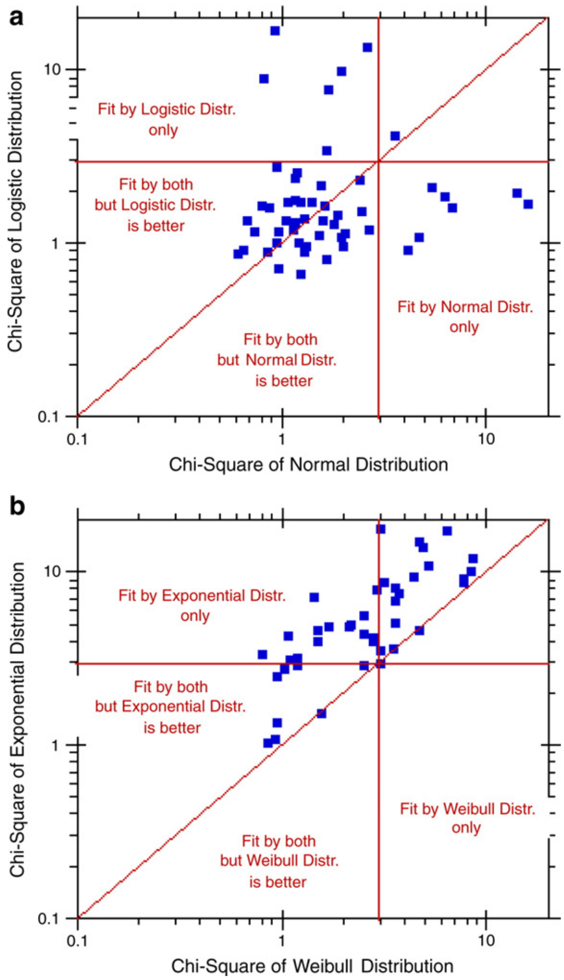

Fig. 4. Chi-square comparison for probability density statistical functions used in the study. a) Fit by normal distribution is compared with logistic, and b) Weibull is compared with exponential distribution.

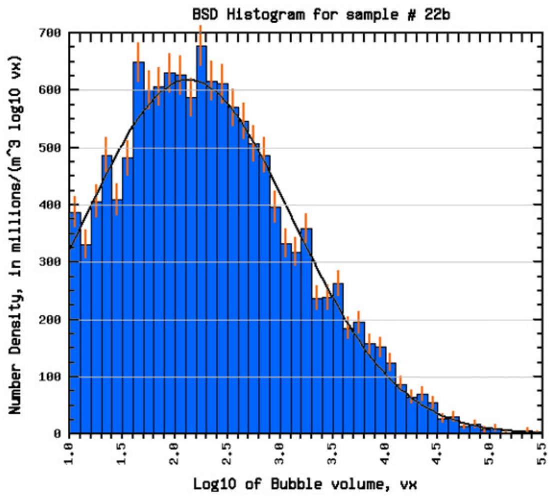

Fig. 5. Visualization of good fit near chi-square subjective threshold value of 3. Normal distribution fit on this graph for sample 22b has chi-square value of 2.5 (see Table 1). Error bars are measurement standard deviation.

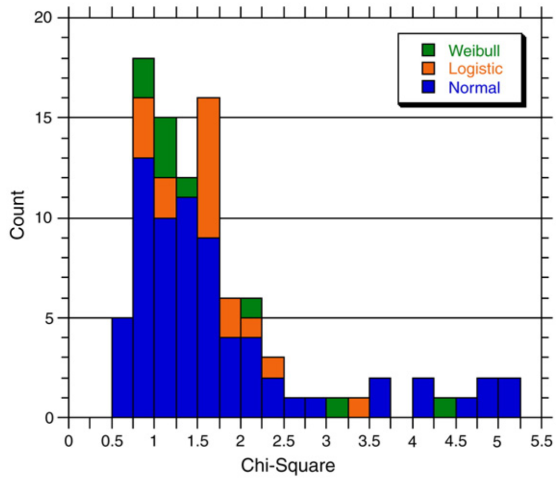

Fig. 6. Histogram of chi-square values for functions that has been chosen to be a best fit in Table 1.

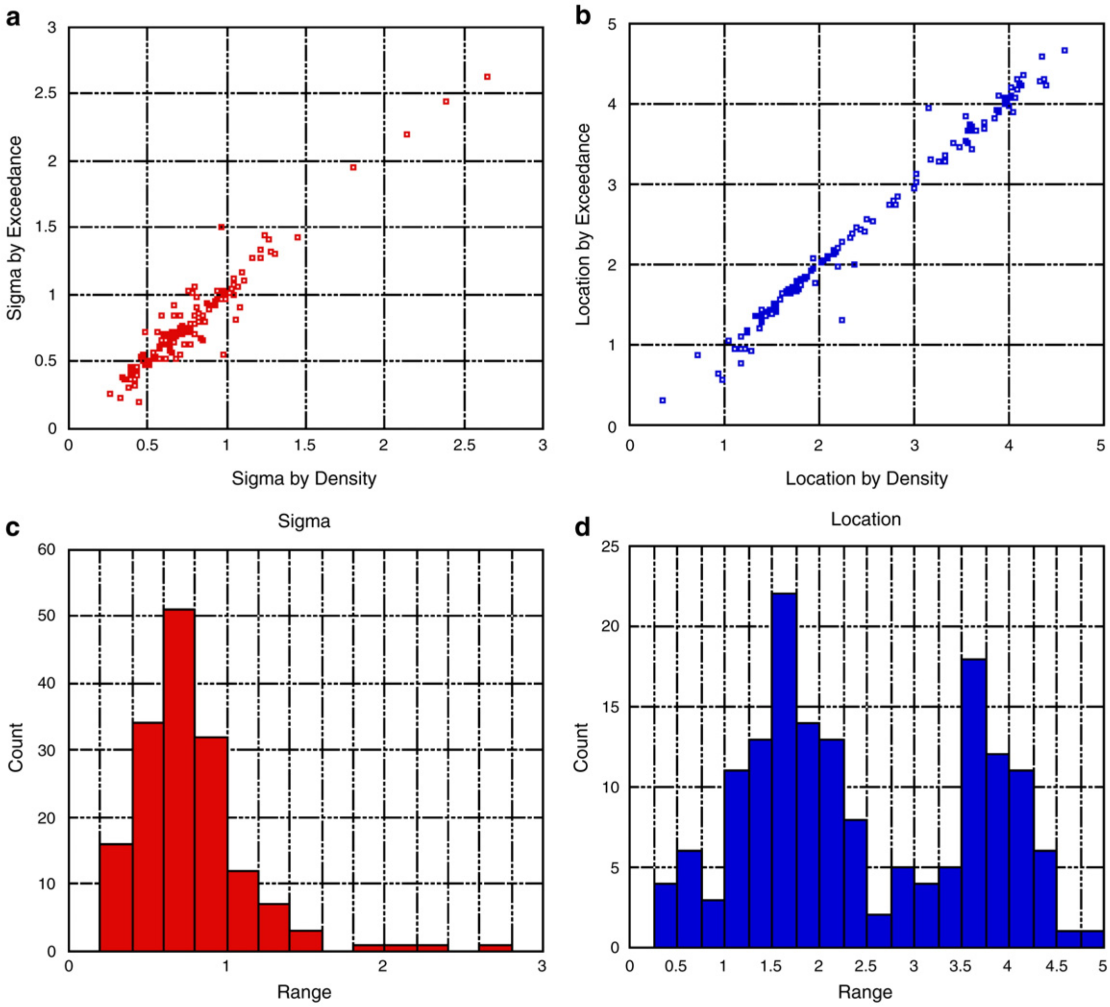

Fig. 7. Comparison of sigma (a) and location (b) values obtained by distribution fit from probability density and exceedance. (c) and (d) are histograms of these parameters. Volume units are in Log 10 voxels (see Fig. 3 for conversions).

Fig. 8 shows BND for both modes. BND for the smaller mode is about one order of magnitude higher than that for the second. These numerical relations for the modes are explored in Section 5.4 below.

5.3. BSD types

We found distinct distribution types in the samples we analyzed (Fig. 9). Within each, they can be grouped into categories with respect to types and values of distribution functions. Each category appears to represent a progressive transition in the shape of the number density graphs, which may reflect different stages within the vesiculation process. Here we can only speculate which processes led to these categories of distribution types. It is likely that nucleation and bubble growth are the primary vesiculation processes operating in basaltic magmas and formed most of the observed monomodal distributions, but second modes in bimodal distributions could be formed by a second nucleation event, Ostwald ripening, or coalescence. The bimodality in our samples was likely produced by second nucleation event and/or coalescence (Sahagian, 1985; Sahagian et al., 1989). We thus consider the most likely scenario for the majority of our samples to be a single or double nucleation/growth event followed by coalescence.

5.3.1. Normal distributions

Normal monomodal distributions comprise about 18% of all analyzed samples. We speculate that these distribution type results from an extended period of bubble growth after a single nucleation event that took place before eruption in the conduit or vent. Fig. 9a displays two examples of this type. Sample 07b is most

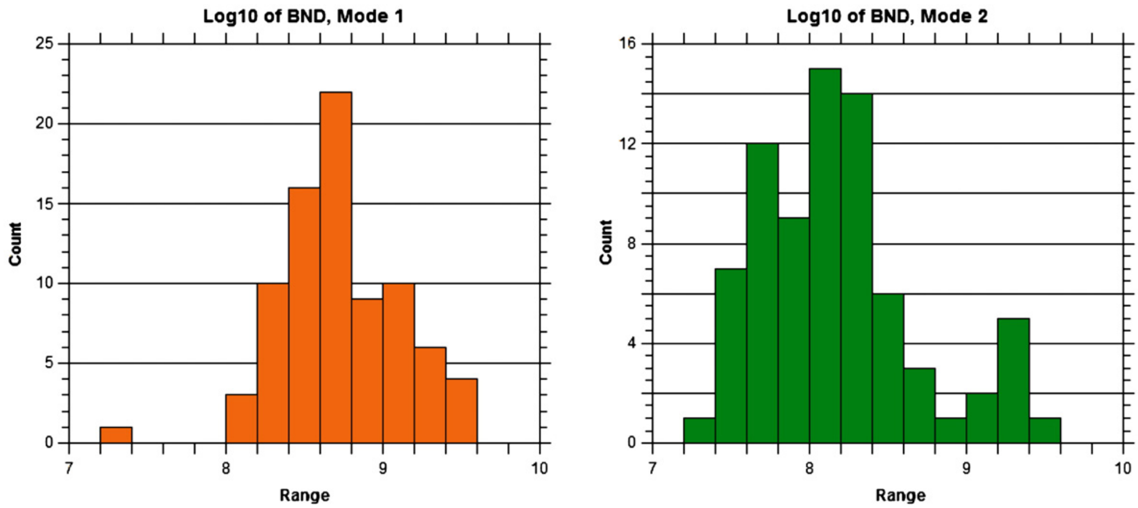

Fig. 8. BND histograms for mode 1 and 2.

typical of this type since its left (small end) wing is cut off due to HRXCT resolution limitations, but fortunately the truncation range for the observed populations can be mathematically found by function minimization routines for the best fit analysis (Proussevitch et al., 2007-this issue, Sections 3 and 9). A nearly complete distribution (sample 32b in Fig. 9a) is a rare case. The purpose for which the samples were originally collected and analyzed only required the position of the mode to be identified, so spurious precision at the small end would have been costly and unnecessary for paleoelevation studies (Sahagian et al., 2002a,b). Normal monomodal distributions resulting from our analyses have modes in the range of 1–2 units, but some samples have higher values (e.g. 32b, 32t) of 3–3.5. Sigma for normal monomodal distributions is about 1 or greater, a higher value than for most other samples (see Fig. 7c). This means that the distributions have a relatively large spread from small to large bubbles.

Normal bimodal distributions are observed in about half of all samples and have wide variations in both mode locations and relative intensity (Fig. 9b–f). Well defined, clearly separated modes of about equal intensity (Fig. 9b) are rare. Keep in mind that relative intensity of the modes should not be confused with relative cumulative bubble volumes since the one from mode 2 is about two orders of magnitude larger than mode 1 volume. Bimodal distributions with non-equivalent mode intensity are more common. These can be closely spaced and have the higher intensity mode to the left or right (Fig. 9c–d). Nevertheless, the majority of normal bimodal distributions have a big difference between mode sizes and the larger size mode has an order of magnitude smaller bubble number density than the small bubbles (Fig. 9e).

In order to be consistent with the nature of normal monomodal distributions (above), we suggest that bimodal distributions are generated by two separate nucleation events with subsequent bubble growth. Since the difference in modal bubble sizes is about two orders of magnitude (Fig. 7d) it is very likely that the larger mode stems from vesiculation in the conduit or vent while the smaller results from vesiculation in lava flows after eruption.

A different type of normal bimodal distributions was found where the two modes are roughly equivalent in amplitude, but not separated far from each other in sizes (Fig. 9f). Sometimes the modes are located so close to each other (sample 38b) that this population could also be fit (with larger error) by other distribution functions (e.g. Weibull). This distribution type appears to be caused by two nucleation events following in quick succession.

5.3.2. Logistic distributions

Basalts with logistic distributions are less common than those with normal distribution and comprise about 20% of all samples.

Logistic monomodal distributions have modes that are barely exposed within our range of observation (Fig. 9g), so that as much as half the bubble population is cut off (sample 25t). Sigma of these distributions appears to be about half of the norm for all other samples.

Logistic bimodal distributions have very similar mode relations as those for normal distributions (Fig. 9h–j), but the mode of large bubbles in logistic distributions usually has much lower number density.

We can only speculate about the genesis of logistic distributions. Nevertheless, considering the fact that power law relations describe the descending part of logistic distributions (Proussevitch et al., 2007-this

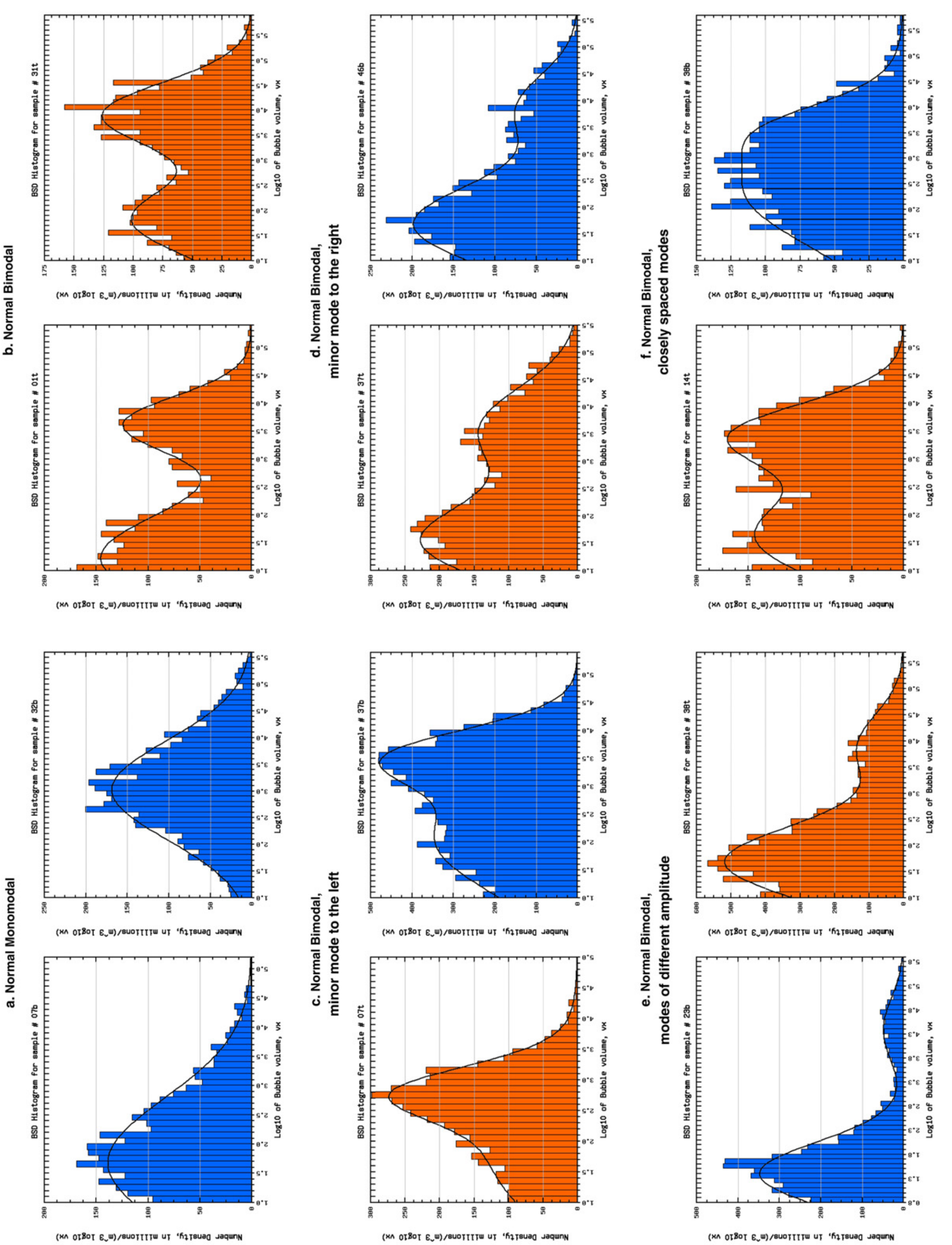
a. Normal Monomodal
b. Normal Bimodal
c. Normal Bimodal, minor mode to the left
d. Normal Bimodal, minor mode to the right
e. Normal Bimodal, modes of different amplitude
f. Normal Bimodal, closely spaced modes
BSD Histogram for sample # 07b
BSD Histogram for sample # 32b
BSD Histogram for sample # 01t
BSD Histogram for sample # 31t
BSD Histogram for sample # 07t
BSD Histogram for sample # 37b
BSD Histogram for sample # 37t
BSD Histogram for sample # 46b
BSD Histogram for sample # 23b
BSD Histogram for sample # 38t
BSD Histogram for sample # 14t
BSD Histogram for sample # 38b
Log10 of Bubble volume, vx
Number Density, in millions/(m^3 log10 vx)

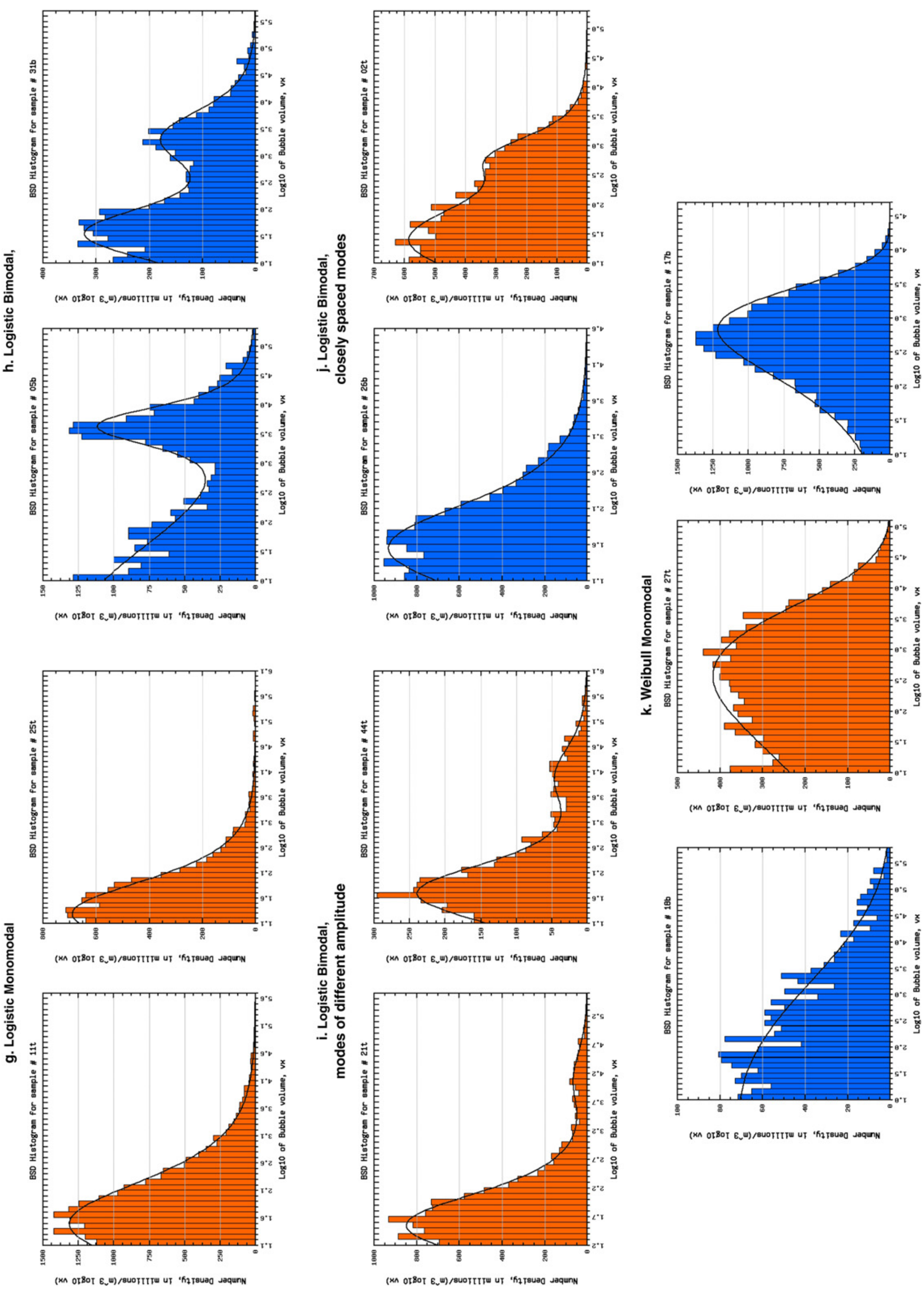

Fig. 9. Some common bubble size distribution types found in Colorado Plateau basalts.

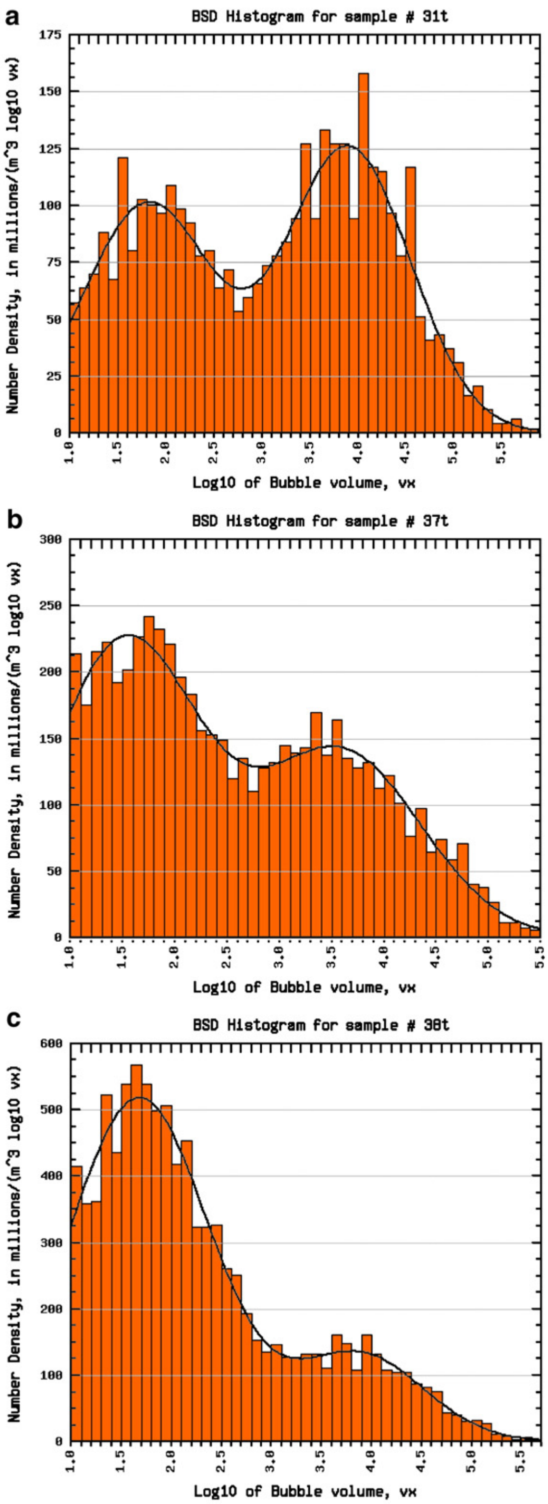

issue) and the former had been often interpreted to reflect coalescence (Gaonac'h et al., 1996b; Blower et al., 2001; Gaonac'h et al., 2005), we can suggest that the logistic distributions are caused by coalescence. This interpretation matches the observation that logistic distributions are the second most common type in quenched crusts of basaltic lava flows (after normal distributions (nucleation-growth)). This follows since coalescence is the second most common vesiculation process in basaltic melts after a combination of nucleation and growth (Blower et al., 2001). The observation that the second mode (large bubbles) of logistic bimodal distributions has much lower number density (Fig. 9i) also agrees with coalescence dynamics, as larger but fewer bubbles result from merging of multiple smaller ones.

5.3.3. Weibull distributions

Weibull monomodal distributions. All Weibull distributions emerging from the basalt samples we analyzed are monomodal. The mode in these distributions commonly represents large bubbles, so in Table 1 it is referred to as mode 2 while mode 1 is reported missing. Examples of these distributions are shown in Fig. 9k. In a few cases the mode represents smaller bubbles (sample 18b) but in those cases, sigma is large, yielding a wide range of bubble sizes.

The mechanism responsible for creating Weibull distributions is not clear. Some might be generated by a single, but prolonged nucleation and growth "event" or by multiple events in quick succession. Given the other distributions and the nature of the Weibull distribution, we consider it unlikely to develop strictly by coalescence. Note the very close resemblance between the graphs for samples 38b and 27t (Fig. 9f and k respectively) suggesting that Weibull distributions of this shape may be formed by multiple nucleation events. For another example, sample 17b appears similar to sample 07t (Fig. 9c and k respectively).

Fig. 10. Possible evolution of two nucleation-growth events taking place in a conduit (mode of larger bubbles) and lava flows (mode of smaller bubbles). Graphs of bimodal normal distributions from (a) to (c) indicate progressive development of post eruptive bubbles in lava flows (mode of smaller bubbles) that could be related to the distance from the vent. Note: examples are samples for the process illustration only that geologically are not related one to each other. Nevertheless, notice that the number density (BND) of the larger mode remains the same for each of those, while BND progressively increases from a to b to c, suggesting that a common process (e.g. pre-eruption vesiculation) founded the larger mode, while different stages of another process (e.g. post-eruption vesiculation) let to the smaller mode.

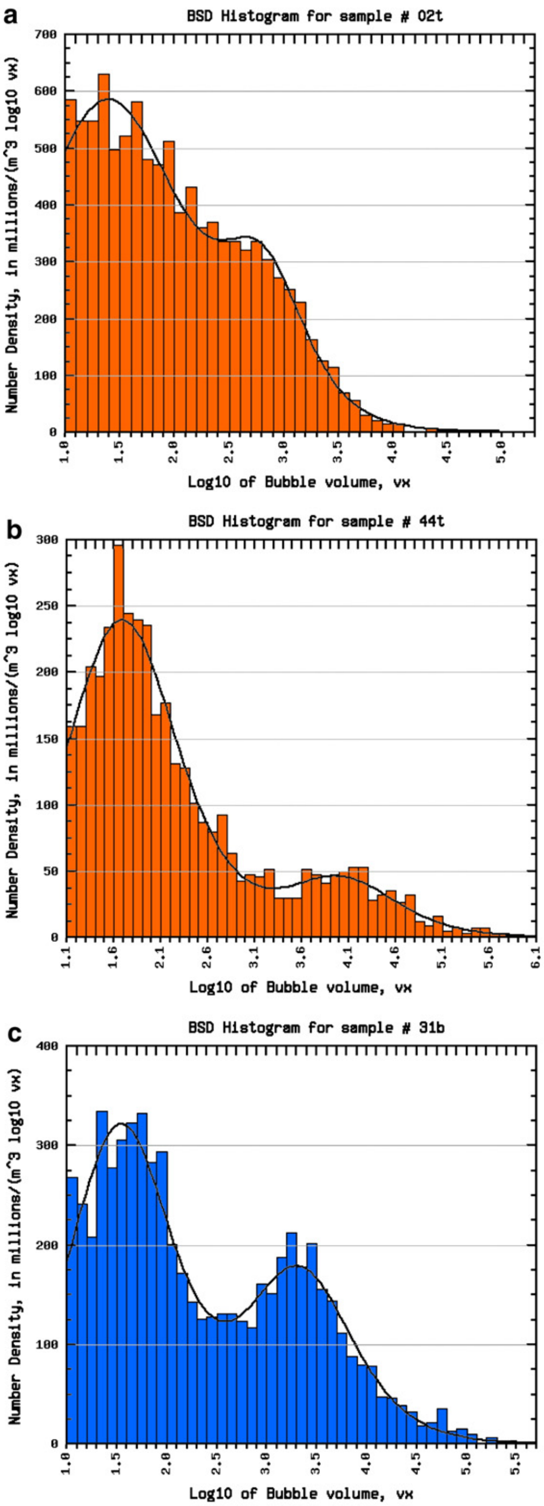

Fig. 11. Possible evolution of distribution types in order from (a) to (c) caused by bubble coalescence. (a) is a logistic bimodal distribution that starts developing the second mode due to coalescence as a side bump on its descending wing. Later it makes better developed second mode (b). As second mode grows we have a clear bimodal distribution (c). Note: samples are not geologically related one to each other.

5.4. Bimodal distributions from coalescence and multiple nucleation events

While it is interesting to speculate about the causes of the various distributions we observe, at this stage, there is no concrete observational mechanistic evidence for a link between magmatic processes and bubble size distributions. The only model results available are already out of date (Sahagian, 1985; Sahagian et al., 1989; Toramaru, 1990), although they do suggest that bimodal distributions can result from coalescence. Nevertheless, it appears that monomodal normal distributions (17 samples out of 96 or about 20% which is one of the most numerous groups) result from a single nucleation and growth event. Its single mode has a characteristic size which has been attributed to a particular growth rate over some characteristic time, with a BND from nucleation rate over the same characteristic time (Marsh, 1988).

Interpretations regarding the causal mechanisms of bimodal distributions are more difficult. The first mode (smaller bubbles) is likely the result of a single nucleation and growth event as in the case of monomodal normal distributions, but the second (larger bubbles) mode may arise from a number of mechanisms such as

- second (earlier in time) nucleation event
- coalescence
- diffusive gas exchange between bubbles (Ostwald ripening)

Ostwald ripening is unlikely to lead to a second mode because a relatively long time is required to significantly change the size distribution (Proussevitch et al., 1993). It is more likely to change the distribution function by skewing the distribution density curve toward the larger bubbles than to create a new mode. Likewise, an extended period of nucleation and growth is not likely to form a discrete second mode, but rather should be expected to lead to a broader distribution than a single short-lived event.

Consequently, for the basalt samples we analyzed the most likely mechanisms for the formation of the second mode are (1) a second nucleation and growth event in case of normal distributions, and (2) coalescence in case of logistic distributions.

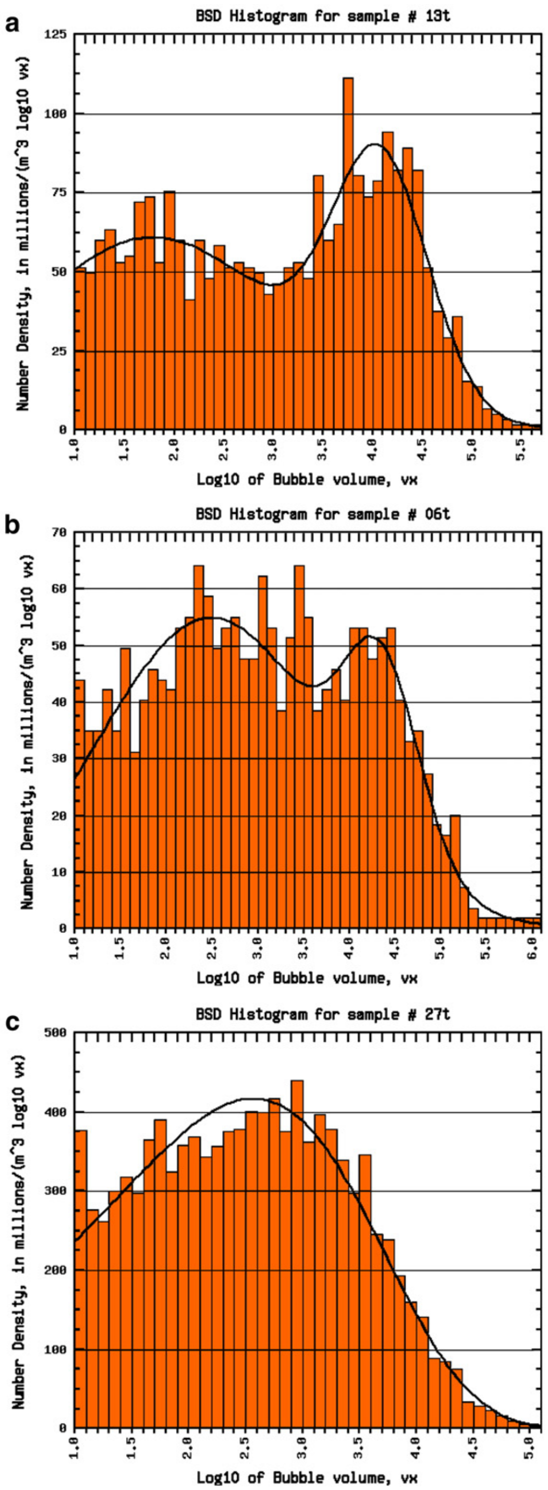

Fig. 12. Possible evolution of multiple nucleation-growth events (a and b) that can lead to Weibull distribution (c). Note: samples are not geologically related to each other.

Fig. 10 illustrates possible progressive evolution of the mode for second nucleation event that represent post eruptive bubbles generated in a lava flow (left mode on the graphs). Presumably this mode develops larger BND as residence time increases with distance from the vent.

In case of bimodal logistic distributions Fig. 11 shows a scenario of evolution of distribution types resulting from coalescence. As coalescence proceeds, a normal mono-modal distribution spawns a second mode that grows from the descending wing (to the larger bubble size of the mode). This develops into an explicit bimodal distribution and as coalescence continues eroding away the first mode. Although this is a conceptual line of evolution, it appears a likely scenario even though no field samples have ever been collected specifically to test it. This, in addition to numerical modeling of coalescence processes is left for future work by us and others.

The coalescence mechanism is supported by the statistical relations of location and intensity (BND) for the two modes observed in our analyzed samples. This can be tested from the standpoint of conservation of gas volume during coalescence. If the second mode is derived from the descending limb of the first mode then the gap should be about as wide as the size of bubbles (since two bubbles coalesce to make a large bubble). Thus the bubbles that used to be at the location of the gap before coalescence have been transformed to the larger but less numerous bubbles of the second mode.

A distinct line of bubble distribution evolution can be caused by multiple nucleation-growth events. The importance of this process has been highlighted in previous work (Blower et al., 2003) which experimentally demonstrated that a combination of superposed multiple nucleation and bubble growth events can lead to a new type of distribution function. Fig. 12 suggests that closely spaced multimodal normal distributions can form a monomodal Weibull distribution as nucleation and growth continues. The right wing slope of the Weibull distribution is very similar to the slope of the larger (by bubble size) mode. As other modes get closer they merge to the single Weibull distribution. Recall that exponential distribution is a special case of Weibull distribution (Proussevitch et al., 2007-this issue) and that the exponential distribution has been shown to be a result of a extended nucleation-growth process (Marsh, 1988).

5.5. Sample vesicularity calculations

A corollary utility of generating distribution functions for bubble populations in volcanic rocks is the ability to integrate them and calculate total void fraction (vesicularity) in the sample (Proussevitch et al., 2007-this issue,

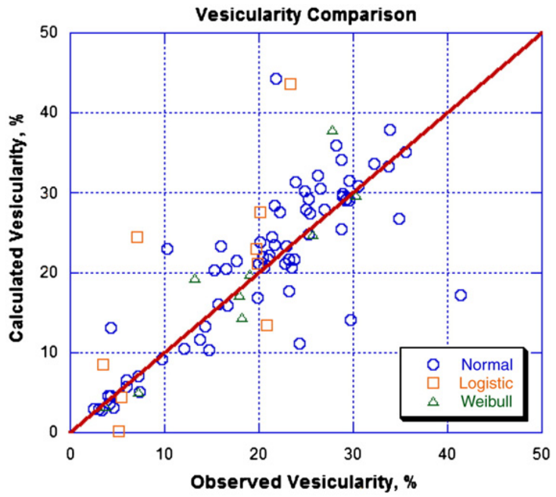

Fig. 13. Comparison of calculated and “observed” vesicularity for the samples from Table 1. Since “observed” vesicularity might not represent the entire population (limited by observation range and sample size), the calculated vesicularity might be more reliable.

Section 8 equations 20–21). HRXCT analysis of samples of course provides the number of void and matrix voxels, and this can be used to calculate vesicularity directly, but in most cases these tallies cannot be accurate because the complete range of bubble sizes is typically not observed in scanned samples, so the population is invariably incomplete (Fig. 9g). In addition, there is a second cause of incomplete populations in observed populations arising from limited sample size that may miss a few of the largest bubbles, and thus severely skew the bulk vesicularity. Integration of the distribution function within the full range of population sizes enables one to circumvent this problem and calculate vesicularity characteristics of the larger-scale lava flow.

Fig. 13 displays a comparison between calculated and “observed” vesicularity of the samples in our collection reported in Table 1. As you can see from the figure, there is a reasonable match for normal and Weibull distributions, where the difference usually does not exceed 5%. The match is not as good for the Logistic distributions discussed above.

6. Conclusions

Analysis of a suite of vesicular basalts demonstrates the applicability of our new statistical analysis to bubble populations generated by high-resolution X-ray computed tomography.

HRXCT provides high-quality data for bubble populations. The resolution routinely achieved by HRXCT allows reliable detection of bubbles as small as 0.1 mm diameter in the 24-mm-diameter cores used in this study; still smaller bubbles could be resolved in smaller-diameter cores. In the cores we utilized, with volumes of ~7.5 cm^3, typical vesicle populations numbered from 5000 to 10,000 bubbles, but reached tens of thousands of bubbles in some instances.

A new statistical analysis (Proussevitch et al., 2007-this issue) has been applied to these bubble populations. Mono- and bimodal functions from the logarithmic family of distributions were tested for all samples. These functions include log normal, log logistic, Weibull, and exponential. A function with best fit was chosen for each sample based on chi-square value (measure of the fit error). Each of the functions fit the data well, and log normal bimodal distributions are most common in our sample suite (Table 2). The remaining (25%) samples are divided between log logistic and Weibull distributions. Exponential distributions are a special case of Weibull distributions with sigma equal to 1.

Our observed distributions (Table 1) have been organized into 11 groups according to type, mode location and intensity. Many of these groups can in turn be combined in three evolutionary trends. We conclude that the first trend reflects evolution from a monomodal normal distribution to bimodal as a result of second nucleation and bubble growth event in a lava flow after its emplacement. The second trend relates to logistic bimodal distributions caused by coalescence. The category follows all stages of this process starting from “nucleation” of the second mode for large bubbles that later develops into a full, well separated, second mode and then ultimately degrades the intensity of the first mode. The third trend shows how a multimodal distribution with closely spaced and superposed modes can result in a monomodal Weibull (e.g. exponential) distribution.

The analytical form of distribution functions for bubble populations can be used to calculate sample vesicularity. In most cases the calculated vesicularity is likely to be more accurate than directly observed (tallied) vesicularity because it integrates all bubble sizes, some of which may be missed in observational population data due to the cutoff of small bubbles by resolution limitations, and of large bubbles due to limited sample size.

An important motivation for this study has been to develop a robust and accurate method to evaluate modal bubble sizes for samples from top and bottom of basaltic flows to be used to find paleoelevation of the flows at the time of their emplacement (Sahagian et al., 2002a,b). The various pairs of samples shown in Table 1 indicate that most modes from tops of flows are larger than their counterparts from the bottoms. In order to use this analysis for paleoelevation, it is necessary to separate pre-eruptive from post-emplacement nucleated bubbles so that only modes of pre-eruptive distributions are used. This application is not in the scope of the present analysis, but is left for future work.

Acknowledgements

This material is based upon work supported by NSF under awards EAR-0207818 and EAR-0509859. The High-Resolution X-ray Computed Tomography Facility at the University of Texas at Austin is supported by NSF grants EAR-0004082 and EAR-0345710.

References

Blower, J.D., Keating, J.P., Mader, H.M., Phillips, J.C., 2001. Inferring volcanic degasing processes from vesicle size distributions. Geophys. Res. Lett. 28 (2), 347–350.

Blower, J.D., Keating, J.P., Mader, H.M., Phillips, J.C., 2003. The evolution of bubble size distributions in volcanic eruptions. J. Volcanol. Geotherm. Res. 120 (1–2), 1–23.

Cashman, K.V., Mangan, M.T., 1994. Physical aspects of magma degassing, II, Constraints on vesiculation processes from textural studies of eruptive products. In: Carroll, M.R., Holloway, J.R. (Eds.), Volatiles in Magmas. Reviews in Mineralogy. Mineral. Soc. of Am., Washington, D. C., pp. 446–478.

Cashman, K.V., Kauahikaua, J.P., 1997. Reevaluation of vesicle distributions in basaltic lava flows. Geology 25, 419–422.

Gaonac'h, H., Lovejoy, S., Stix, J., Scherzter, D., 1996a. A scaling growth model for bubbles in basaltic lava flows. Earth Planet. Sci. Lett. 139, 395–409.

Gaonac'h, H., Stix, J., Lovejoy, S., 1996b. Scaling effects on vesicle shape, size and heterogeneity of lavas from Mount Etna. J. Volcanol. Geotherm. Res. 74 (1–2), 131–153.

Gaonac'h, H., Lovejoy, S., Schertzer, D., 2005. Scaling vesicle distributions and volcanic eruptions. Bull. Volcanol. 67 (4), 350–357.

Ketcham, R., Carlson, W., 2001. Acquisition, optimization and interpretation of X-ray computed tomographic imagery: applications to the geosciences. Comput. Geosci. 27, 381–400.

Marsh, B.D., 1988. Crystal size distributions (CSD) in rocks and the kinetics and dynamics of crystallization: 1. Theory. Contr. Min. Pet. 99, 277–291.

Oh, W., Lindquist, W.B., 1999. Image thresholding by indicator kriging. IEEE Trans. Pattern Anal. Mach. Intell. 21, 590–602.

Proussevitch, A., Sahagian, D., Kutolin, V., 1993. Stability of foams in silicate melts. J. Volcanol. Geotherm. Res. 59, 161–178.

Proussevitch, A.A., Sahagian, D.L., 2001. Recognition and separation of discrete objects within complex 3D voxelized structures. Comput. Geosci. 27, 441–454.

Proussevitch, A.A., Sahagian, D.L., Tsentalovich, E.P., 2007-this issue. Statistical analysis of bubble and crystal size distributions: Formulations and procedures. J. Volcanol. Geotherm. Res. doi:10.1016/j.jvolgeores.2007.04.007.

Sahagian, D.L., 1985. Bubble migration and coalescence during the solidification of basaltic lava flows. J. Geol. 93, 205–211.

Sahagian, D.L., Anderson, A.T., Ward, B., 1989. Bubble coalescence in basalt flows: comparison of a numerical model with natural examples. J. Volcanol. Geotherm. Res. 52, 49–56.

Sahagian, D.L., Proussevitch, A.A., 1998. 3D Particle size distributions from 2D observations: stereology for natural applications. J. Volcanol. Geotherm. Res. 84, 173–196.

Sahagian, D.L., Proussevitch, A.A., Carlson, W., 2002a. Timing of Colorado Plateau uplift: initial constraints from vesicular basalt-derived paleoelevations. Geology 30 (9), 807–810.

Sahagian, D.L., Proussevitch, A.A., Carlson, W.D., 2002b. Analysis of vesicular basalts and lava emplacement processes for application as a paleobarometer/paleoaltimeter. J. Geol. 110, 671–685.

Sarda, P., Graham, D., 1990. Mid-ocean ridge popping rocks: implication for degassing at ridge crests. Earth Planet. Sci. Lett. 97, 268–289.

Shin, H., Lindquist, W.B., Sahagian, D.L., Song, S.R., 2005. Analysis of the vesicular structure of basalts. Comput. Geosci. 31 (4), 473–487.

Toramaru, A., 1990. Measurement of bubble size distributions in vesiculated rocks with implications for quantitative estimation of eruption processes. J. Volcanol. Geotherm. Res. 43, 71–90.